Received: 10 November 2017 | Revised: 11 January 2018 | Accepted: 8 February 2018

DOI: 10.1111/psyp.13072

ORIGINAL ARTICLE

WILEY PSYCHOPHYSIOLOGY SPR SOCIETY FOR PSYCHOPHYSIOLOGICAL RESEARCH

Toward a better noninvasive assessment of preejection period: A novel automatic algorithm for B-point detection and correction on thoracic impedance cardiogram

Mohamad Forouzanfar[1,2] | Fiona C. Baker[1] | Massimiliano de Zambotti[1] | Corey McCall[2] | Laurent Giovangrandi[2] | Gregory T. A. Kovacs[1,2]

[1] Center for Health Sciences, SRI International, Menlo Park, California, USA

[2] Transducers Lab, Department of Electrical Engineering, Stanford University, Stanford, California, USA

Correspondence
Mohamad Forouzanfar, SRI International, 333 Ravenswood Ave., Menlo Park, CA 94025, USA.
Email: mohamad.forouzanfar@sri.com

Funding information
National Institutes of Health (grant HL103688) (to F. C. B.), (grant R21-AA024841) (to I. M. C. and M. de Z.), Natural Sciences and Engineering Research Council of Canada (grant PDF-454018-2014) (to M. F.)

Abstract

Impedance cardiography is the most common clinically validated, noninvasive method for determining the timing of the opening of the aortic valve, an important event used for measuring preejection period, which reflects sympathetic beta-adrenergic influences on the heart. Automatic detection of the exact time of the opening of the aortic valve (B point on the impedance cardiogram) has proven to be challenging as its appearance varies between and within individuals and may manifest as a reversal, inflection, or rapid slope change of the thoracic impedance derivative's (dZ/dt) rapid rise. Here, a novel automatic algorithm is proposed for the detection of the B point by finding the main rapid rise of the dZ/dt signal, which is due to blood ejection. Several conditions based on zero crossings, minima, and maxima of the dZ/dt signal and its derivatives are considered to reject any unwanted noise and artifacts and select the true B-point location. The detected B-point locations are then corrected by modeling the B-point time data using forward and reverse autoregressive models. The proposed algorithm is validated against expert-detected B points and is compared with different conventional methods; it significantly outperforms them by at least 54% in mean error, 30% in mean absolute error, and 27% in standard deviation of error. This algorithm can be adopted in ambulatory studies requiring beat-to-beat evaluation of cardiac hemodynamic parameters over extended time periods where expert scoring is not feasible.

KEYWORDS

algorithm, autoregressive model, B-point detection, cardiovascular system, impedance cardiography, preejection period

1 | INTRODUCTION

Impedance cardiography (ICG) is a noninvasive method for evaluating the electromechanical properties of the heart. ICG records fluctuations in electrical impedance in the upper thorax when an AC current is applied (Sherwood et al., 1990). The basal impedance signal (Z_0) and the rate of change in the impedance on a given beat (dZ/dt) are recorded, usually in combination with electrocardiography (ECG), which allows the determination of the onset of ventricular depolarization (Sherwood et al., 1990; Visser, Mook, van der Wall, & Zijlstra, 1993). ICG is used to estimate stroke volume as well as systolic time intervals including preejection period (PEP) and left ventricular ejection time. PEP represents the time interval between the beginning of ventricular depolarization (Q wave on the ECG) and the opening of the aortic valve (B point on the dZ/dt impedance signal), when left ventricular blood ejection occurs (Pinheiro, Postolache, & Girão, 2013; Tavakolian, 2016). PEP is important in psychophysiology research because it is considered a

valid index of myocardial contractility and beta-adrenergic sympathetic control of the heart (Bagley & El-Sheikh, 2014; Cacioppo et al., 1994; Schächinger, Weinbacher, Kiss, Ritz, & Langewitz, 2001; Sherwood, Allen, Obrist, & Langer, 1986).

ICG is considered superior to other noninvasive techniques for measuring PEP, such as those that rely on external carotid pulse measurement, since it is a more direct method and is associated with measurement error at only two points: Q wave and B point (Szilagyi, Lang, & Balazs, 1992). Carotid pulse measurement must be accompanied by phonocardiography to provide an estimate of the aortic valve opening time (Tavel, 1985) and has been found unreliable due to the nonlinear phase shift between the root aortic and external carotid pulses (Lewis, Rittogers, Froester, & Boudoulas, 1977).

Several automatic approaches exist for the accurate detection of ECG Q wave (Arzeno, Deng, & Poon, 2008; Berntson, Lozano, Chen, & Cacioppo, 2004). However, the exact point of the opening of the aortic valve (B point) has proven to be extremely difficult to automatically detect from beat-to-beat variation of thoracic impedance due to the distorting effect of body movements, muscle contractions, respiration, higher frequency noise, and different cardiovascular pathologies on the shape of the dZ/dt signal, leading to variability in dZ/dt morphology between and within individuals (Árbol et al., 2017; Miller & Horvath, 1978; Sherwood et al., 1990). Therefore, expert visual inspection is usually required to detect the correct B-point location, which is very time consuming and inefficient when analyzing data collected over extended time periods (van Lien, Schutte, Meijer, & de Geus, 2013). For example, 1 hr of data from an individual with a heart rate of 60 bpm would require the manual determination of the B-point location for 3,600 cardiac cycles.

Different approaches have been developed for the automatic detection of dZ/dt B point (see Table 1). Most of these are sensitive to noise and artifact and may fail when there are several reversals, inflections, and rapid slope changes on the dZ/dt rise. Methods based on ensemble averaging of the dZ/dt signal over several cardiac cycles have been proposed (Cieslak et al., 2015; Kelsey & Guethlein, 1990; Kelsey et al., 1998; Muzi et al., 1985; Riese et al., 2003; Shoemaker, Appel, Kram, Nathan, & Thompson, 1988) to reduce the effect of noise and artifacts. However, such approaches are not appropriate for beat-to-beat analysis of cardiac hemodynamics parameters. Moreover, the accurate detection of B point on the dZ/dt ensemble average may still remain challenging. Árbol et al. (2017) provided visual guidlines to facilitate the manual detection of B point in various dZ/dt morphologies. However, no automatic algorithm was proposed for the detection of the B point. There is a need to develop automatic algorithms for the beat-to-beat detection of dZ/dt B point that are less sensitive to noise and artifact and are more robust to the variability in dZ/dt signal morphology.

The focus of this article is the demonstration of a novel analytic approach to improve the automatic detection of the dZ/dt B point and thus increase the reliability of measuring PEP and sympathetic nervous system activity via ICG without the need for expert visual scoring. Considering that blood ejection manifests as the main rise in the dZ/dt signal, a new B-point detection algorithm is proposed based on identifying the most prominent monotonically increasing segment of the dZ/dt signal and searching for the B point within that segment. Several conditions based on the amplitude, zero crossings, and local minima and maxima of the dZ/dt and its derivatives are considered in the rejection of noise and artifacts and the correct detection of B-point location. Detected B points that are too close to or too far from neighboring points in either time or amplitude are identified using an outlier detection algorithm and are corrected using forward and reverse autoregressive models derived from their neighboring points. The performance of the proposed algorithm is illustrated with several examples and is compared against expert visually detected B points and several conventional algorithms applied to a pilot data set collected from 20 individuals. To explore the robustness of different algorithms to physiological variabilities and the artifacts caused by changes in breathing rate and pattern, the performance of the proposed algorithm was evaluated during both resting baseline and postexercise recovery conditions.

2 | METHOD

2.1 | Experimental design

This study was approved by the institution review boards of Stanford University (Protocol ID 37133) and SRI International (Protocol ID W33Y7J). Data were collected from 20 participants (14 men and 6 women), ranging in age from 22 to 63 years, with no history of cardiovascular disease. Written informed consent was obtained from each participant before the experiments.

ICG was obtained using a commercialized device (HIC-2000, Microtronics, Old Greenwich, CT) using a spot electrode configuration. The upper voltage electrode was placed at the base of the neck and the lower voltage electrode on the thorax at the level of the xiphisternal junction. The current electrodes were placed on the upper part of the neck and the lower region of the rib cage approximately 3 cm away from the voltage electrodes (Bacon, Keller, Lavoie, & Campbell, 2010; Sherwood, Royal, Hutcheson, & Turner, 1992). ECG was obtained using a custom-designed circuit. The standard Lead II ECG signal was acquired by placing three electrodes, one each on the right wrist, left wrist, and left leg of the participant.

TABLE 1 Comparison of different ICG B-point detection algorithms

B-point detection algorithm	Pros	Cons
Zero crossing of dZ/dt before dZ/dt maximum (C point) (Sherwood et al., 1990)	Can be relatively easily implemented as it does not require any complex processing	Fails when dZ/dt signal drifts due to respiration or body movements
Reversal (local minimum) of dZ/dt before the C point (Stern, Wolf, & Belz, 1985)	Works well for normal patterns of dZ/dt	The B point may appear as an inflection or rapid slope change after the last local minimum or reversal of dZ/dt
Maximum of the d^2Z/dt^2 before the C point (Debski et al., 1991)	Can be used when there is no clear B point on dZ/dt rapid rise	Sensitive to noise Maximum of the d^2Z/dt^2 corresponds to the dZ/dt highest slope that usually occurs after the B point
Maximum of the d^2Z/dt^2 in a 50-ms time window starting 150 ms before the C point (Árbol et al., 2017)	Can be used when there is no clear B point on dZ/dt rapid rise Not sensitive to any noise and artifacts that occur outside the chosen window	Maximum of the d^2Z/dt^2 corresponds to the dZ/dt highest slope that usually occurs after the B point Still sensitive to noise and artifacts that happen within the chosen window The chosen time windows may not be universally applicable
Reversal (local minimum) of d^2Z/dt^2 before the C point (Debski et al., 1993)	Detects the inflection point of dZ/dt	Sensitive to noise Does not work when B point appears as a rapid slope change or when there are several inflection points on dZ/dt rapid rise
Maximum of d^3Z/dt^3 signal before the C point (Debski et al., 1993)	Detects the rapid slope change of dZ/dt	Sensitive to noise Does not work when there are several inflection and rapid slope changes on dZ/dt rapid rise
Maximum of d^3Z/dt^3 signal within 300 ms before the C point (Árbol et al., 2017)	Detects the rapid slope change of dZ/dt Not sensitive to noise outside the window	Does not work when there are several inflection and rapid slope changes on dZ/dt rapid rise Still sensitive to noise and artifacts that happen within the chosen window The chosen time windows may not be universally applicable
Data-driven polynomial model between the ECG R-peak and B-point interval and the R-peak and C-point interval (Lozano et al., 2007)	Does not require direct detection of B point Performs well when there are several reversals, inflections, and rapid slope changes on dZ/dt rapid rise	Sensitive to any noise and artifact that alters the location of the C point May be sensitive to abnormal or noisy ECG Data-driven models may need to be tuned for different health conditions or age groups that have not been seen before
Machine learning algorithms trained over user selected B-point patterns (Cieslak et al., 2017)	After being trained, does not require direct detection of B point	Sensitive to any noise and artifact causing patterns similar to the B point on dZ/dt signal Needs to be retrained for different patterns of B point that have not been seen before
Time-frequency analysis (Wang, Sun, & Van de Water, 1995)	Capable of detecting all the changes in dZ/dt	Sensitive to any artifacts that have overlapping frequency content with that of the dZ/dt around B point
Wavelet analysis (Shyu, Lin, Liu, & Hu, 2004)	Extracts features from dZ/dt in different resolutions	Sensitive to any artifacts that have overlapping frequency content with that of the dZ/dt around B point Computationally expensive

Sensor outputs were connected to differential analog inputs of a multiplexing analog to digital converter (NI USB-6251 Data Acquisition System, National Instruments Co., Austin, TX). The NI USB-6251 channel delay is of the order of 10 μs. Given that the magnitude of PEP is of the order of 100 ms, the channel delay is nonsignificant. The signals were sampled at 2 kHz with a resolution of 16 bits. Custom software was used to capture the signals and store them in a computer for further analysis. All the algorithms were designed in MATLAB R2017a (MathWorks, Inc., Natick, MA).

Two minutes of baseline data were recorded while the participant was sitting comfortably on a chair, breathing normally. While still seated, the participant was then asked to pedal a miniexerciser bike, which was placed under their feet for 2 min. Two minutes of postexercise data were collected.

Simultaneously recorded ICG and ECG signals from the 20 participants, at rest and postexercise, were processed for analysis. The dZ/dt signal was first digitally filtered with a 4th-order Butterworth band-pass filter to remove the high frequency noise and artifacts and low frequency drift. The lower and upper cutoff frequencies were set to 0.5 Hz and 40 Hz, respectively. The filter was applied in both forward and backward directions to avoid any phase shift.

2.2 | Development of the automatic algorithm

A novel algorithm was developed based on the detection of the most prominent monotonically increasing segment of the dZ/dt signal and searching for the B point within that segment. To avoid any unwanted artifact, the search for the monotonically increasing segments were limited between the local minimum of dZ/dt signal that occurred before its rapid rise (A point) and the dZ/dt maximum (C point). The C point was detected using an automatic peak detection algorithm available in MATLAB R2017a software. The A point was detected as the local minimum within one third of the beat-to-beat interval prior to the C point. The monotonically increasing segments of the dZ/dt signal within the search interval were then detected according to d^2Z/dt^2 sign change. Any segment with positive d^2Z/dt^2 is monotonically increasing while any segment with negative d^2Z/dt^2 is monotonically decreasing. The prominence of a monotonically increasing segment was determined according to its height and location. The monotonically increasing segment with the highest height that started from at least half of C-point amplitude and reached at least two thirds of C-point amplitude was selected as the most prominent, and the B point was searched over this segment. Figure 1 shows different patterns of dZ/dt signal where the detection of B point is challenging along with the detected most prominent monotonically increasing segment of dZ/dt signal in red.

If there were no significant inflections or rapid slope changes on the most prominent monotonically increasing segment of dZ/dt, the first point of the segment that corresponded to a local minimum or reversal of dZ/dt was selected as the B point. If there were any significant inflections or rapid slope changes on this segment, the last significant one that occurred within the first third of the segment was assigned as the B point. Inflection points were detected as the zero crossings of the d^3Z/dt^3 with a negative to positive sign change (i.e., when d^3Z/dt^3 was zero and d^2Z/dt^2 was greater than zero). The rapid slope changes were detected as the local maximums of the d^3Z/dt^3. The significance of an inflection was determined according to dZ/dt slope at that point given by d^2Z/dt^2 value. The significant inflection points were those at which the value of d^2Z/dt^2 was less than a threshold that was set to $10\times H/f_s$, where H is the dZ/dt height defined as the amplitude difference between A point and C point and f_s is the sampling frequency. The significance of a rapid slope change was determined according to d^3Z/dt^3 value with respect to H. The significant rapid slope changes were those points at which the value of d^3Z/dt^3 was greater than a threshold that was set to $4\times H/f_s$. These two thresholds determined the sensitivity of the proposed algorithm to inflections and rapid slope changes in dZ/dt signal.

To further correct the detected B points, an outlier detection algorithm was employed to identify the B points that occur too early or too late compared to the rest of the data points. Forward and reverse autoregressive models were then derived from the rest of the data points to correct the outliers.

To detect outliers and perform autoregressive modeling, the B-point time data needs to be stationarized (Hamilton, 1994). The B-point time data baseline was first obtained using a 4th-order Butterworth low-pass filter with a cutoff frequency of 0.1 Hz. The filter was applied in both forward and backward directions to avoid any phase shift. The stationarized B-point time data were then obtained by subtracting the baseline from the original time data. The outliers were detected as those points that were three times the scaled median absolute deviation away from the median (Rousseeuw & Leory, 2005). Forward and backward autoregressive models were then fitted to the remaining points. The order of models were chosen by minimizing the Akaike information criterion (Hirotugu, 1969). The maximum length of prediction to find the optimal model was set to 60 s. The forward and backward autoregressive model parameters were obtained recursively using the Burg's method (Kay, 1988). The outlier corrected values were extrapolated from the derived autoregressive models. Each outlier value was obtained as the weighted average of the values estimated by forward and backward prediction. The baseline was subsequently added back to the data. This process was repeated until no more outliers were detected.

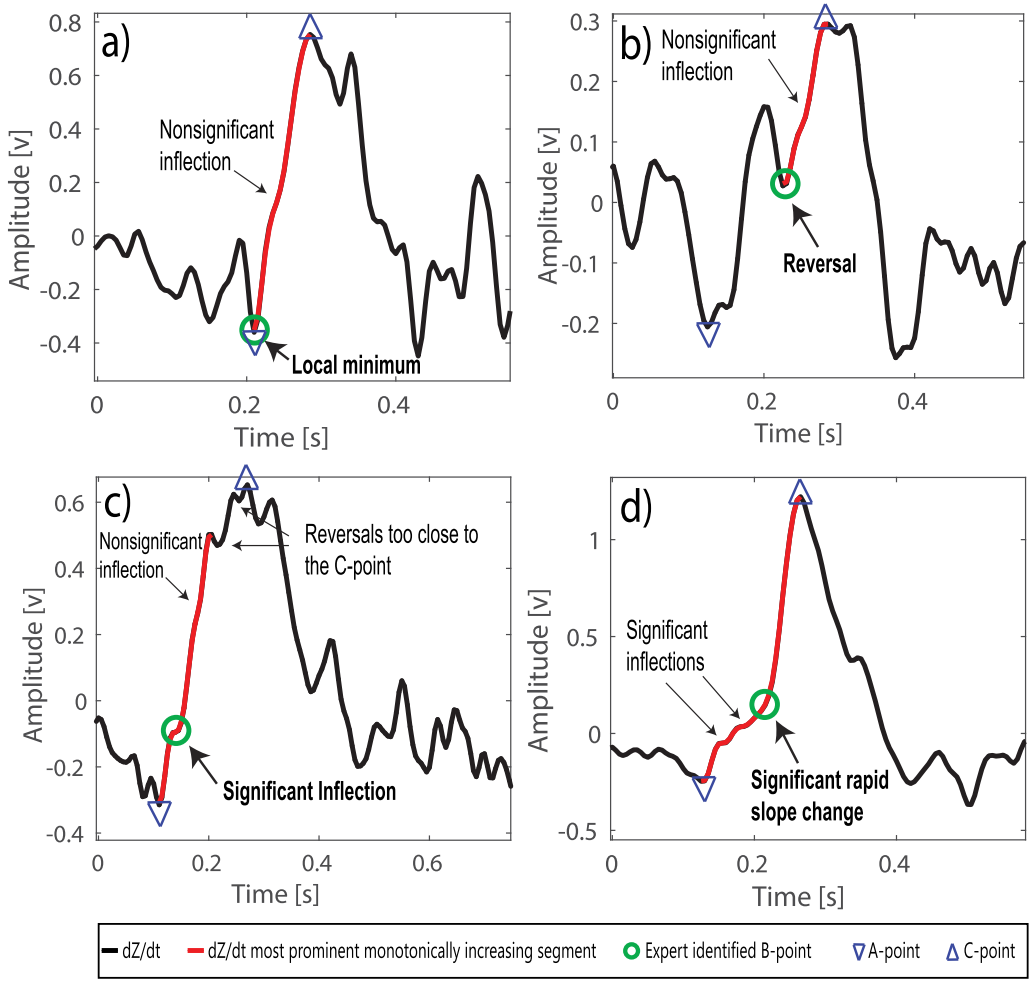

FIGURE 1 Example of challenging patterns of the dZ/dt signal showing variability in B-point appearance: B point exhibited as (a) a local minimum, (b) a reversal, (c) an inflection, (d) a rapid slope change at the beginning of the dZ/dt main rise. The A point (minimum) and C point (maximum) are marked by downward and upward blue triangles, respectively. The expert-identified B point is marked by a green circle. The most prominent monotonically increasing segment of dZ/dt signal is highlighted in red

Examples of outlier detection and correction using the proposed algorithm are shown in Figure 2.

The proposed algorithm can be summarized as follows:

Step 1: Detection

1. Detect the main dZ/dt peak (C point).
2. Find the main local minimum (A point) within one third of the beat-to-beat interval before the C point.
3. Calculate the dZ/dt height (H) as the amplitude difference between the detected A point and C point.
4. Find all the monotonically increasing segments between A point and C point and select the one with the highest height that starts from at least half of the C-point amplitude and reaches at least two thirds of C-point amplitude.
5. Find all the d^3Z/dt^3 zero crossings over the first third of the detected most prominent monotonically increasing segment and discard those with dZ/dt slope (d^2Z/dt^2) of greater than $10\times H/f_s$.
6. Find all the d^3Z/dt^3 local maximums over the first third of the most prominent monotonically increasing segment and discard those with d^3Z/dt^3 value of less than $4\times H/f_s$.
7. Label the last zero crossing or local maximum of d^3Z/dt^3 as the B point. If no zero crossing or local maximum exists, label the first point of the segment as B point.

Step 2: Correction

1. Estimate the B-point time data baseline using a 4th-order Butterworth low-pass filter with a cutoff frequency of 0.1 Hz.
2. Stationarize the fiducial point time data by subtracting the low pass trend from the original time data.
3. Detect the outliers of the stationarized B-point time data. Outliers are defined as the points that are three times the scaled median absolute deviation away from the median.
4. Estimate the correct values of the outliers using forward and reverse autoregressive modeling.

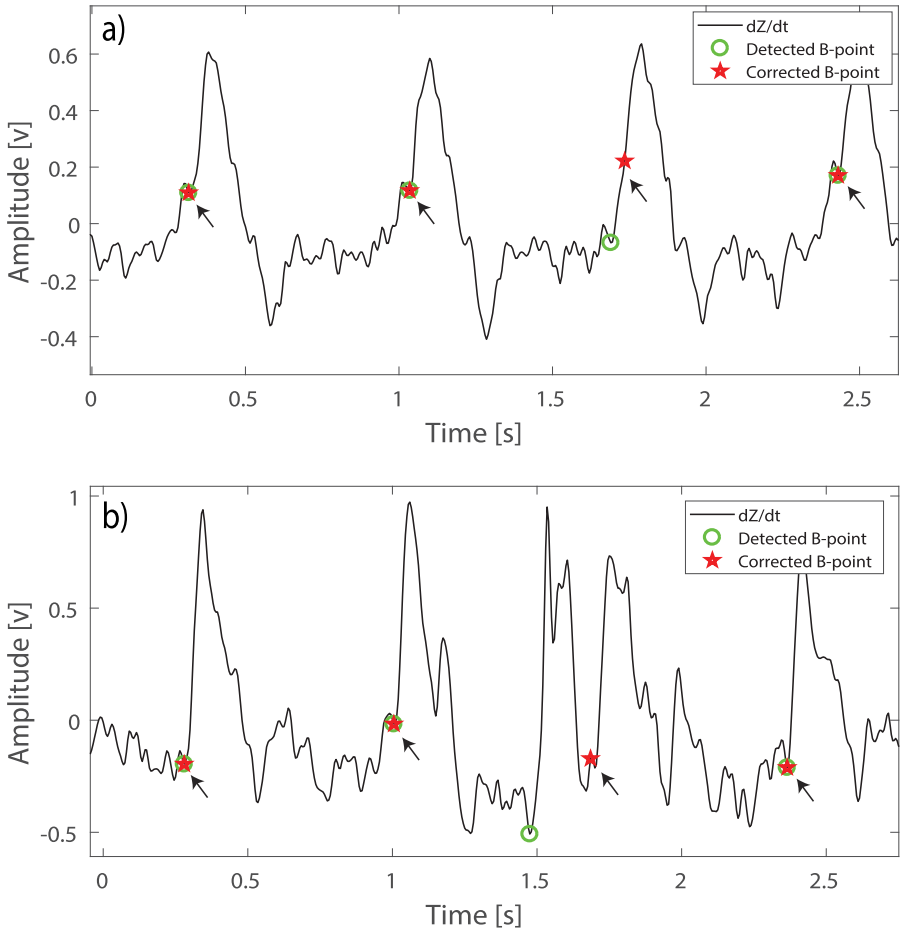

FIGURE 2 Examples of outlier detection and correction using the proposed algorithm. The detected and corrected B points are marked by green circles and red stars, respectively. The expert visually detected B points are shown by black arrows

5. Add the baseline back to the corrected stationarized time series.
6. Repeat the process until no more outliers are detected.

2.3 | Data analysis

In addition to the proposed algorithm, three common conventional methods based on the detection of zero crossing (Sherwood et al., 1990), reversal point (Stern, Wolf, & Belz, 1985), and third-derivative maximum (Árbol et al., 2017) of dZ/dt signal were implemented. The dZ/dt zero crossing and reversal point are traditional B-point detection methods that are still widely used in the literature because of their simplicity and potential for automatization (Ermishkin, Kolesnikov, & Lukoshkova, 2014). The d^3Z/dt^3 maximum is more appropriate when the detection of B point is challenging and has been found to outperform the traditional techniques in such cases (Árbol et al., 2017). The locations of B points as identified visually by an expert were considered as reference values. The expert (M. de Z.), who has several years of experience in recording and analyzing different cardiovascular signals including ICG and ECG (de Zambotti et al., 2013, 2014; de Zambotti, Covassin, Cellini, Sarlo, & Stegagno, 2012; de Zambotti, Covassin, Cellini, Sarlo, Torre, & Stegagno, 2012; de Zambotti, Covassin, De Min Tona, Sarlo, & Stegagno, 2011), was blind to the developed algorithms and considered the visual B-point detection guidelines provided in Árbol et al., 2017, and Sherwood et al., 1990, along with the previous and next cardiac cycle dZ/dt patterns and ECG R-peak timings to determine the true B-point location.

The performance of different B-point detection algorithms was evaluated in terms of mean error (ME), mean absolute error (MAE), and standard deviation of error (SDE) relative to the reference. Error was defined as the algorithm minus the expert-detected B-point time. The error metrics were calculated for each participant across all cardiac cycles. A set of Bonferroni-corrected paired samples *t* tests were performed to compare the proposed algorithm's estimation error with the others.

To further evaluate the performance of different B-point detection algorithms, PEP was calculated as the time difference between the ICG B point and the ECG Q-wave onset.

TABLE 2 Performance comparison of different B-point detection algorithms in terms of ME, MAE, and SDE relative to reference across 20 participants

	Error (ms)	dZ/dt zero crossing	dZ/dt reversal	d^3Z/dt^3 maximum	Proposed algorithm
Baseline	ME	−21.3	−19.4	29.0	8.6
	MAE	26.0	20.8	34.0	12.2
	SDE	29.2	16.0	16.1	11.2
Postexercise	ME	−24.8	−14.9	36.8	6.9
	MAE	25.8	17.1	36.8	12.0
	SDE	22.2	16.1	16.2	11.7

Note. ME = mean error; MAE = mean absolute error; SDE = standard deviation of error.

TABLE 3 *T*-test results comparing error of the proposed algorithm with that of the others

Algorithm	Baseline	Postexercise
dZ/dt zero crossing	$t(19) = -4.65$, $p = .0002$ Cohen's $d = 1.34$	$t(19) = -6.61$, $p = .0000$ Cohen's $d = 1.79$
dZ/dt reversal	$t(19) = -5.66$, $p = .0000$ Cohen's $d = 2.03$	$t(19) = -5.08$, $p = .0001$ Cohen's $d = 1.35$
d^3Z/dt^3 maximum	$t(19) = 14.18$, $p = .0000$ Cohen's $d = 1.47$	$t(19) = 10.81$, $p = .0000$ Cohen's $d = 2.09$

The Q-wave onset was detected as the last point before the ECG R peak where the slope falls below a threshold. The threshold was set to $-1.2 \times R_{peak}/f_s$, where f_s is the ECG sampling frequency and R_{peak} is the R-peak amplitude. R peak was detected using a peak detection algorithm available in MATLAB R2017a software. PEP was averaged across all cardiac cycles for each participant. The PEPs obtained by different algorithms were compared with the reference (PEP derived from expert-identified B points) using a set of Bonferroni-corrected paired samples *t* tests.

Pearson correlation analysis was performed to compare the strength of the association between the estimated PEP values from each algorithm and the reference.

3 | RESULTS

Table 2 lists the average ME, MAE, and SDE for different B-point detection algorithms relative to the reference for 20 participants. The proposed algorithm performed well at

TABLE 4 Comparison of PEP averaged across 2 min of cardiac cycles for 20 participants at baseline and postexercise obtained by different B-point detection algorithms

	Preejection period parameters (ms)	dZ/dt zero crossing	dZ/dt reversal	d^3Z/dt^3 maximum	Proposed algorithm	Expert reference
Baseline	PEP mean	103.2	105.2	153.5	133.1	124.5
	PEP standard deviation	31.2	33.4	22.8	19.6	23.7
	PEP minimum	41.9	62.2	125.8	76.4	87.0
	PEP maximum	175.1	169.1	205.2	169.3	173.4
Postexercise	PEP mean	81.7	91.7	143.4	113.5	106.6
	PEP standard deviation	25.8	29.7	18.9	24.3	25.1
	PEP minimum	41.4	53.6	117.7	75.1	72.5
	PEP maximum	135.0	153.7	186.4	153.0	159.1

TABLE 5 *T*-test results comparing the different algorithm PEP estimates and the reference

Algorithm	Baseline	Postexercise
dZ/dt zero crossing	$t(19) = -3.40$, $p = .0030$	$t(19) = -4.07$, $p = .0006$
dZ/dt reversal	$t(19) = -3.81$, $p = .0012$	$t(19) = -3.71$, $p = .0015$
d^3Z/dt^3 maximum	$t(19) = 11.29$, $p = .0000$	$t(19) = 10.81$, $p = .0000$
Proposed algorithm	$t(19) = 2.66$, $p = .0155$	$t(19) = 2.17$, $p = .0428$

baseline and postexercise, showing the lowest ME, MAE, and SDE among all B-point detection algorithms. The ME, MAE, and SDE of the proposed algorithm are lower than of the others by at least 58%, 41%, and 30%, respectively, in the baseline, and by at least 54%, 30%, and 27%, respectively, in postexercise recovery condition. The Bonferroni-corrected paired samples *t* tests with adjusted alpha levels of .0167 (.05/3) confirmed that these improvements are statistically significant, with large effect sizes (see Table 3).

Table 4 lists the PEP mean, standard deviation, minimum, maximum, ME, and SDE obtained by different algorithms during baseline and postexercise recovery conditions obtained across the 20 participants. The reference values obtained from the expert visually detected B points are also listed in the last column. The proposed algorithm consistently performed better than other algorithms by achieving the closest PEP mean and standard deviation to the reference. The Bonferroni-corrected paired samples *t* tests with adjusted alpha levels of .0125 (.05/4) confirmed that the proposed algorithm's PEP estimates are not significantly different from the reference (see Table 5). The rest of the algorithm PEP estimates were significantly different from the reference.

Considering that the normal PEP range varies from 70 ms to 175 ms (Árbol et al., 2017), the expert- and the proposed algorithm-derived PEP values reported in Table 4 are within the normal range. On the other hand, the d^3Z/dt^3 maximum algorithm overestimates the PEP while the dZ/dt reversal and zero-crossing algorithms underestimate the PEP.

Figure 3 shows the PEP trend averaged across participants during baseline and postexercise recovery conditions. The PEP time trend was obtained by evenly interpolating the PEP values for each participant over the 2-min measurement period and averaging the PEP values across the 20 participants. As expected, the PEP is reduced from the baseline condition to postexercise recovery. In the postexercise condition, all the algorithms also show a similar increasing trend in PEP over time that matches the expert-derived PEP as well. However, the proposed algorithm most closely tracks the reference PEP during both baseline and postexercise recovery conditions.

The correlation analysis revealed that the proposed algorithm PEP estimates have the highest correlation with the reference in both baseline and postexercise recovery conditions. The Pearson correlation coefficients during baseline and

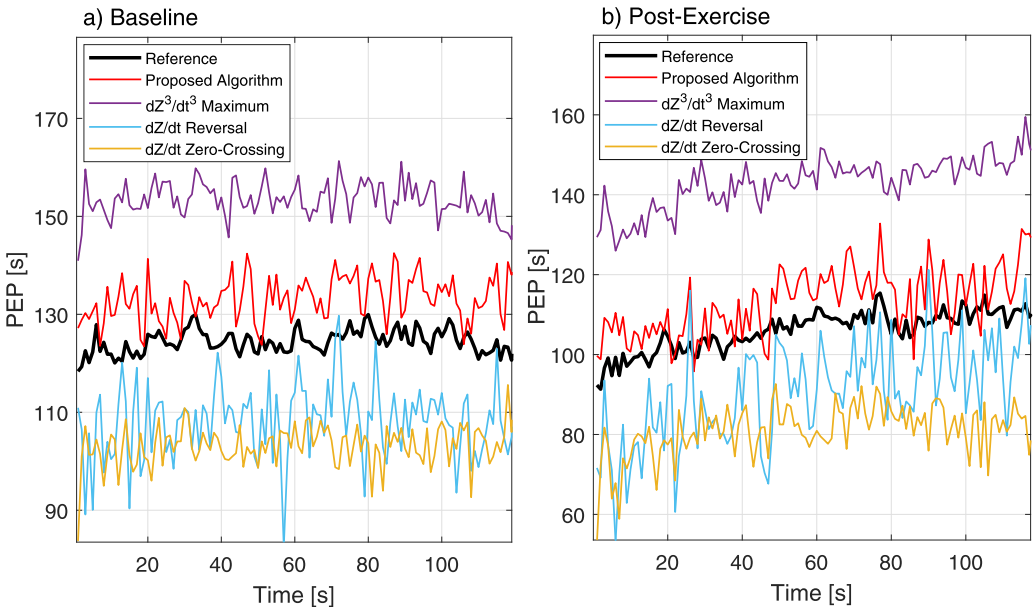

FIGURE 3 Average PEP pattern derived from different algorithms used to detect the B point during (a) 2-min baseline, and (b) 2-min postexercise recovery conditions in 20 participants

postexercise conditions were, respectively, 0.93 and 0.88 for the proposed algorithm, 0.87 and 0.73 for d^3Z/dt^3 maximum algorithm, 0.86 and 0.77 for dZ/dt reversal algorithm, and 0.46 and 0.67 for dZ/dt zero-crossing algorithm.

The strength of the correlation between all the algorithms (except the zero-crossing algorithm) and the reference was lower in the postexercise recovery condition than baseline mainly due to the higher level of breathing and movement artifacts affecting the detection algorithms.

4 | DISCUSSION

Accurate detection of aortic valve opening is important in psychophysiology and cardiovascular research. The most common noninvasive approach for detecting the aortic valve opening is based on analyzing the rate of change in thoracic impedance (dZ/dt). However, automatic detection of the exact time of the aortic valve opening (B point on dZ/dt) is challenging as the dZ/dt pattern changes between and within individuals and therefore expert visual scoring is usually required. In this article, we proposed a new automatic algorithm for the detection and correction of B point in dZ/dt signal that is robust to the variations of dZ/dt signal and outperforms the conventional algorithms.

The main disadvantage of the conventional B-point detection algorithms is that they are based on fixed rules for the detection of B point. Such rules are based on the detection of the zero crossing (Sherwood et al., 1990), reversal point (Stern, Wolf, & Belz, 1985), inflection (Debski, Zhang, Jennings, & Kamarck, 1993), or rapid slope change (Árbol et al., 2017; Debski et al., 1993) of the dZ/dt signal. However, it has been observed that B point could appear as any such points, and its appearance could change between individuals and within individuals from beat to beat (Árbol et al., 2017). Using a fixed rule for the detection of B point results in large estimation errors as reported in Table 2 and 3. Figure 1 shows examples of the dZ/dt signal where B point appears as a local minimum, reversal, inflection, or rapid slope change over the dZ/dt rapid rise. It can be observed that a fixed rule for the detection of B point may succeed in one case and fail in other cases.

One of the advantages of the proposed algorithm over the conventional algorithms is that it does not follow a fixed B-point detection rule. Instead, several conditions are used to detect the correct minimum, reversal, inflection, or rapid slope change of the dZ/dt rapid rise that corresponds to the true aortic valve opening time. These characteristic points are detected from the first three derivatives of the dZ/dt signal, and threshold values are used to limit the selection to the most significant ones. Figure 1 shows examples of significant and nonsignificant inflection and rapid slope changes.

Another disadvantage of prior B-point detection methods is their sensitivity to noise, movement artifact, and respiration. Since blood ejection causes the main change in thoracic impedance, we limited the search for the B point over dZ/dt most prominent monotonically increasing segment. This avoids any noise and artifact outside this segment affecting the detection algorithm. Moreover, by limiting the search for the B point over the first one third of this segment, we eliminate the effect of any noise and artifact that may occur later on the dZ/dt rise. Figure 1c shows an example of the dZ/dt signal where several reversals and inflections happen near the peak (C point), none of which are the true B point.

Several conditions were also considered for the detection of the most prominent monotonically increasing segment of dZ/dt signal to avoid the selection of any rapid rise that is due to movement artifacts. The search for the most prominent monotonically increasing segment of dZ/dt signal was only limited between the dZ/dt local minimum (A point) and its main maximum (C point). It was also ensured that such segments start from at least half of the C-point amplitude and reach at least two thirds of the C-point amplitude. Figure 1b shows an example of dZ/dt signal where two monotonically increasing segments exist, and while the first one has higher height, the second is selected as the most prominent one based on the described conditions.

The proposed algorithm has several advantages over other methods. Unlike the zero-crossing method (Sherwood et al., 1990), the proposed algorithm is not sensitive to dZ/dt signal drifts. Unlike dZ/dt reversal (Stern et al., 1985), d^2Z/dt^2 reversal (Debski et al., 1993), d^2Z/dt^2 maximum (Árbol et al., 2017; Debski et al., 1991), and d^3Z/dt^3 maximum (Árbol et al., 2017; Debski et al., 1993) methods that are only based on the detection of the reversal, rapid slope change, highest slope, or inflection of the dZ/dt signal before the C point, the proposed algorithm considers all such characteristic points on dZ/dt rapid rise to detect the true B-point location. Unlike the data-driven model between ECG R peak and dZ/dt B and C points (Lozano et al., 2007), the proposed algorithm is not sensitive to the noise and artifacts that alter the location of the C point or R peak. Unlike the machine learning methods (Cieslak et al., 2017), the proposed algorithm does not require a training data set representing all possible patterns of B point. Compared to the time-frequency (Wang, Sun, & Van de Water, 1995) and wavelet analysis (Wang et al., 1995) methods, the proposed algorithm has less complexity and is less sensitive to noise and artifacts that have overlapping frequency content with that of the dZ/dt around B point.

While the proposed rules aim to reduce the effects of noise and artifacts, there could still be cases where they fail. Examples of such cases are shown in Figure 2. Figure 2a shows dZ/dt signal over four consecutive cardiac cycles where the B-point appearance changed over the third cardiac

cycle from a significant to a nonsignificant inflection and therefore was not correctly detected. Figure 2b shows the case where a very high-level movement artifact or noise caused a rapid rise on dZ/dt signal that was mistaken as the rapid rise caused by cardiac ejection. In such cases, the proposed correction algorithm reassigns the detected B points based on their neighboring point pattern of occurrence. Such incorrectly detected B points will have timings that are too short or too long compared to the rest of the detected B points and therefore can be identified by an outlier detection algorithm. By modeling the time pattern of the B points using an autoregressive algorithm, such outliers can be corrected. The proposed correction algorithm can play a crucial role in the detection of B-point location when no identifiable change appears on the rise of dZ/dt signal or the B point is buried under a high level of noise. In such cases, even a reliable visual scoring of the B point is impossible, and therefore such portions of data must be excluded in any study.

About 5% of the cardiac cycles in our data set were detected as outliers and corrected using the proposed correction method. Therefore, the outlier correction algorithm did not have a significant effect on the overall reported results. However, for beat-to-beat studies where the cardiac hemodynamic parameter variability is studied over time, such outlier detection and correction methods become crucial. The proposed outlier detection and correction algorithm was tested on the other methods as well. It did not correct the overall bias of such methods; however, it could correct their individual outliers.

The performance of the proposed algorithm was evaluated in baseline and postexercise recovery conditions. During the postexercise recovery condition, the dZ/dt signal pattern changes due to different physiological variabilities, which allowed us to better verify the robustness of the algorithm to such dZ/dt pattern variabilities. The proposed algorithm consistently performed better than prior methods even during the postexercise condition. All methods showed a decrease in PEP in the postexercise recovery condition relative to baseline, likely reflecting increased sympathetic activity to the heart in association with exercise. Here, we have focused on developing a method to accurately detect the B point and thus calculate PEP. However, it should be kept in mind that there are other issues with the interpretation of PEP, regardless of accuracy of measurement, such as the influence of the afterload on PEP independent of beta-adrenergic control (Newlin & Levenson, 1979), which needs to be corrected (Trinder et al., 2001) in psychophysiology studies.

The proposed algorithm was evaluated on a relatively small data set collected from 20 participants during resting baseline and postexercise recovery conditions. The data set comprised all healthy participants, and no patients with complicated dZ/dt patterns such as those with known arteriosclerosis were included. Future work will involve validating the proposed algorithm on a larger number of healthy participants as well as patients with different cardiovascular diseases. The proposed algorithm was experimentally compared with three prior methods based on the detection of zero crossing (Sherwood et al., 1990), reversal point (Stern et al., 1985), and third-derivative maximum (Árbol et al., 2017) of dZ/dt signal. Future work should focus on comparing the proposed algorithm with other state-of-the-art methods listed in Table 1.

A major limitation of the proposed B-point detection algorithm is its sensitivity to any noise and artifacts that may cause a rapid rise like those caused by blood ejection between the dZ/dt A and C points. The proposed method is also sensitive to any noise and artifact that changes the dZ/dt signal pattern during its rapid rise. However, such outliers are mostly detected and corrected by the proposed B-point correction algorithm as shown in Figure 2b. The proposed B-point correction method will work well when the majority of the B points is detected correctly and therefore the pattern of the B-point time data can be accurately estimated from these points using the autoregressive forward and backward models.

It is important that the proposed algorithm can still be used in applications where assessment of aortic opening time regardless of ECG timing is desired. Using ECG as an additional source of information can further improve the proposed detection and correction algorithms by narrowing the search interval for the B point, which will be addressed in future work.

Using other simultaneously recorded cardiovascular signals may further improve the detection of true B-point location. For example, in Nederend, Ten Harkel, Blom, Berntson, and de Geus, 2017, simultaneously recorded transthoracic echocardiography was used to derive the criterion to select the true B point out of several candidates on the dZ/dt signal. Phonocardiogram may also be used to improve the B-point detection. While the phonocardiogram alone may not be a reliable marker of the exact aortic valve opening (Tavel, 1985), its S1 component can be used as additional source of information to narrow the search interval for the B point or to find the B-point selection criterion when there are several candidates.

The proposed algorithm was based on offline processing of the recorded data. Future work will also focus on real-time algorithms that can detect the B point and measure PEP as data are streaming. In conclusion, the proposed algorithm performed better than three conventional algorithms both under resting condition and during postexercise recovery. The proposed automatic algorithm can be applied when large amounts of data are collected and expert visual scoring is not possible.

ACKNOWLEDGMENTS

This research was partly supported by the National Institutes of Health, HL103688 (to F. C. B.) and R21-AA024841 (to M. de Z.) and the Natural Sciences and Engineering Research Council of Canada, PDF-454018-2014 (to M. F.). NIH grant R21-AA024841 was also awarded to Ian M. Colrain, SRI International, Menlo Park, CA. The content is solely the responsibility of the authors and does not necessarily represent the official views of the National Institutes of Health and the Natural Sciences and Engineering Research Council of Canada. Authors are working to make their software freely available. Please contact the corresponding author for any enquiries.

ORCID

Mohamad Forouzanfar http://orcid.org/0000-0001-8849-0144

REFERENCES

Árbol, J. R., Perakakis, P., Garrido, A., Mata, J. L., Fernández-Santaella, M. C., & Vila, J. (2017). Mathematical detection of aortic valve opening (B point) in impedance cardiography: A comparison of three popular algorithms. *Psychophysiology*, *54*, 350–357. https://doi.org/10.1111/psyp.12799

Arzeno, N. M., Deng, Z. D., & Poon, C. S. (2008). Analysis of first-derivative based QRS detection algorithms. *IEEE Transactions on Biomedical Engineering*, *55*, 478–484. https://doi.org/10.1109/TBME.2007.912658

Bacon, S. L., Keller, A. J., Lavoie, K. L., & Campbell, T. S. (2010). Comparison of a three-quarter electrode band configuration with a full electrode band configuration for impedance cardiography. *Psychophysiology*, *47*, 1087–1093. https://doi.org/10.1111/j.1469-8986.2010.01010.x

Bagley, E. J., & El-Sheikh, M. (2014). Relations between daytime pre-ejection period reactivity and sleep in late childhood. *Journal of Sleep Research*, *23*, 337–340. https://doi.org/10.1111/jsr.12117

Berntson, G. G., Lozano, D. L., Chen, Y. J., & Cacioppo, J. T. (2004). Where to Q in PEP. *Psychophysiology*, *41*, 333–337. https://doi.org/10.1111/j.1469-8986.2004.00156.x

Cacioppo, J., Berntson, G., Binkley, P., Quigley, K., Uchino, B., & Fieldstone, A. (1994). Autonomic cardiac control. II. Noninvasive indices and basal response as revealed by autonomic blockades. *Psychophysiology*, *31*, 586–598.

Cieslak, M., Ryan, W. S., Babenko, V., Erro, H., Rathbun, Z. M., Meiring, W., … Grafton, S. T. (2017). Quantifying rapid changes in cardiovascular state with a moving ensemble average. *Psychophysiology*. Advance online publication. https://doi.org/10.1111/psyp.13018

Cieslak, M., Ryan, W. S., Macy, A., Kelsey, R. M., Cornick, J. E., Verket, M., … Grafton, S. (2015). Simultaneous acquisition of functional magnetic resonance images and impedance cardiography. *Psychophysiology*, *52*, 481–488. https://doi.org/10.1111/psyp.12385

de Zambotti, M., Cellini, N., Baker, F. C., Colrain, I. M., Sarlo, M., & Stegagno, L. (2014). Nocturnal cardiac autonomic profile in young primary insomniacs and good sleepers. *International Journal of Psychophysiology*, *93*, 332–339. https://doi.org/10.1016/j.ijpsycho.2014.06.014

de Zambotti, M., Covassin, N., Cellini, N., Sarlo, M., & Stegagno, L. (2012). Cardiac autonomic profile during rest and working memory load in essential hypotensive women. *International Journal of Psychophysiology*, *85*, 200–205. https://doi.org/10.1016/j.ijpsycho.2012.05.002

de Zambotti, M., Covassin, N., Cellini, N., Sarlo, M., Torre, J., & Stegagno, L. (2012). Hemodynamic and autonomic modifications during sleep stages in young hypotensive women. *Biological Psychology*, *91*, 22–27. https://doi.org/10.1016/j.biopsycho.2012.05.009

de Zambotti, M., Covassin, N., De Min Tona, G., Sarlo, M., & Stegagno, L. (2011). Sleep onset and cardiovascular activity in primary insomnia. *Journal of Sleep Research*, *20*, 318–325. https://doi.org/10.1111/j.1365-2869.2010.00871.x

de Zambotti, M., Covassin, N., Sarlo, M., De Min Tona, G., Trinder, J., & Stegagno, L. (2013). Nighttime cardiac sympathetic hyperactivation in young primary insomniacs. *Clinical Autonomic Research*, *23*, 49–56. https://doi.org/10.1007/s10286-012-0178-2

Debski, T. T., Kamarck, T. W., Jennings, J. R., Young, L. W., Eddy, M. J., & Zhang, Y. X. (1991). A computerized test battery for the assessment of cardiovascular reactivity. *International Journal of Bio-Medical Computing*, *27*, 277–289. https://doi.org/10.1016/0020-7101(91)90068-P

Debski, T. T., Zhang, Y., Jennings, J. R., & Kamarck, T. W. (1993). Stability of cardiac impedance measures: Aortic opening (B-point) detection and scoring. *Biological Psychology*, *36*, 63–74.

Ermishkin, V. V., Kolesnikov, V. A., & Lukoshkova, E. V. (2014). Age-dependent and pathologic changes in ICG waveforms resulting from superposition of pre-ejection and ejection waves. *Physiological Measurement*, *35*, 943–963. https://doi.org/10.1088/0967-3334/35/6/943

Hamilton, J. D. (1994). *Time series analysis*. Princeton, NJ: Princeton University Press.

Hirotugu, A. (1969). Fitting autoregressive models for prediction. *Annals of the Institute of Statistical Mathematics*, *21*, 243–247. https://doi.org/10.1007/bf02532251

Kay, S. M. (1988). *Modern spectral estimation: Theory and application*. Englewood Cliffs, NJ: Prentice Hall.

Kelsey, R. M., & Guethlein, W. (1990). An evaluation of the ensemble averaged impedance cardiogram. *Psychophysiology*, *27*, 24–33. https://doi.org/10.1111/j.1469-8986.1990.tb02173.x

Kelsey, R. M., Reiff, S., Wiens, S., Schneider, T. R., Mezzacappa, E. S., & Guethlein, W. (1998). The ensemble-averaged impedance cardiogram: An evaluation of scoring methods and interrater reliability. *Psychophysiology*, *35*, 337–340. https://doi.org/10.1037/e526132012-264

Lewis, R. P., Rittogers, S. E., Froester, W. F., & Boudoulas, H. (1977). A critical review of the systolic time intervals. *Circulation*, *56*, 146–158. https://doi.org/10.1161/01.CIR.56.2.146

Lozano, D. L., Norman, G., Knox, D., Wood, B. L., Miller, B. D., Emery, C. F., & Berntson, G. G. (2007). Where to B in dZ/dt.

Psychophysiology, *44*, 113–119. https://doi.org/10.1111/j.1469-8986.2006.00468.x

Miller, J. C., & Horvath, S. M. (1978). Impedance cardiography. *Psychophysiology*, *15*, 80–91. https://doi.org/10.1111/j.1469-8986.1978.tb01340.x

Muzi, M., Ebert, T. J., Tristani, F. E., Jeutter, D. C., Barney, J. A., & Smith, J. J. (1985). Determination of cardiac output using ensemble-averaged impedance cardiograms. *Journal of Applied Physiology*, *58*, 200–205. https://doi.org/10.1152/jappl.1985.58.1.200

Nederend, I., Ten Harkel, A. D. J., Blom, N. A., Berntson, G. G., & de Geus, E. J. C. (2017). Impedance cardiography in healthy children and children with congenital heart disease: Improving stroke volume assessment. *International Journal of Psychophysiology*, *120*, 136–147. https://doi.org/10.1016/j.ijpsycho.2017.07.015

Newlin, D., & Levenson, R. (1979). Pre-ejection period: measuring beta-adrenergic influences upon the heart. *Psychophysiology*, *16*, 546–553. https://doi.org/10.1111/j.1469-8986.1979.tb01519.x

Pinheiro, E., Postolache, O., & Girão, P. (2013). Contactless impedance cardiography using embedded sensors. *Measurement Science Review*, *13*, 157–164. https://doi.org/10.2478/msr-2013-0025

Riese, H., Groot, P. F., van den Berg, M., Kupper, N. H., Magnee, E. H., Rohaan, E. J., … de Geus, E. J. (2003). Large-scale ensemble averaging of ambulatory impedance cardiograms. *Behavior Research Methods, Instruments, & Computers*, *35*, 467–477. https://doi.org/10.3758/bf03195525

Rousseeuw, P. J., & Leory, A. M. (2005). *Robust regression and outlier detection*. New York, NY: John Wiley & Sons.

Schächinger, H., Weinbacher, M., Kiss, A., Ritz, R., & Langewitz, W. (2001). Cardiovascular indices of peripheral and central sympathetic activation. *Psychosomatic Medicine*, *63*, 788–796. https://doi.org/10.1097/00006842-200109000-00012

Sherwood, A., Allen, M. T., Fahrenberg, J., Kelsey, R. M., Lovallo, W. R., & Doornen, L. J. P. (1990). Methodological guidelines for impedance cardiography. *Psychophysiology*, *27*, 1–23. https://doi.org/10.1111/j.1469-8986.1990.tb02171.x

Sherwood, A., Allen, M. T., Obrist, P. A., & Langer, A. W. (1986). Evaluation of beta-adrenergic influences on cardiovascular and metabolic adjustments to physical and psychological stress. *Psychophysiology*, *23*, 89–104. https://doi.org/10.1111/j.1469-8986.1986.tb00602.x

Sherwood, A., Royal, S. A., Hutcheson, J. S., & Turner, J. R. (1992). Comparison of impedance cardiographic measurements using band and spot electrodes. *Psychophysiology*, *29*, 734–741. https://doi.org/10.1111/j.1469-8986.1992.tb02051.x

Shoemaker, W. C., Appel, P. L., Kram, H. B., Nathan, R. C., & Thompson, J. L. (1988). Multicomponent noninvasive physiologic monitoring of circulatory function. *Critical Care Medicine*, *16*(5), 482–490. https://doi.org/10.1097/00003246-198805000-00004

Shyu, L. Y., Lin, Y. S., Liu, C. P., & Hu, W. C. (2004). The detection of impedance cardiogram characteristic points using wavelet transform. *Computers in Biology and Medicine*, *34*, 165–175. https://doi.org/10.1016/s0010-4825(03)00040-4

Stern, H. C., Wolf, G. K., & Belz, G. G. (1985). Comparative measurements of left ventricular ejection time by mechano-, echo- and electrical impedance cardiography. *Arzneimittel-Forschung*, *35*, 1582–1586.

Szilagyi, N., Lang, E., & Balazs, L. (1992). Computer determination of systolic time intervals based on impedance cardiography. *International Journal of Psychophysiology*, *13*, 45–49. https://doi.org/10.1016/0167-8760(92)90019-8

Tavakolian, K. (2016). Systolic time intervals and new measurement methods. *Cardiovascular Engineering and Technology*, *7*, 118–125. https://doi.org/10.1007/s13239-016-0262-1

Tavel, M. E. (1985). *Clinical phonocardiography and external pulse recording*: Chicago, IL: Year Book Medical Publishers.

Trinder, J., Kleiman, J., Carrington, M., Smith, S., Breen, S., Tan, N., & Kim, Y. (2001). Autonomic activity during human sleep as a function of time and sleep stage. *Journal of Sleep Research*, *10*, 253–264. https://doi.org/10.1046/j.1365-2869.2001.00263.x

van Lien, R., Schutte, N. M., Meijer, J. H., & de Geus, E. J. (2013). Estimated preejection period (PEP) based on the detection of the R-wave and dZ/dt-min peaks does not adequately reflect the actual PEP across a wide range of laboratory and ambulatory conditions. *International Journal of Psychophysiology*, *87*, 60–69. https://doi.org/10.1016/j.ijpsycho.2012.11.001

Visser, K. R., Mook, G. A., van der Wall, E., & Zijlstra, W. G. (1993). Theory of the determination of systolic time intervals by impedance cardiography. *Biological Psychology*, *36*, 43–50. https://doi.org/10.1016/0301-0511(93)90079-n

Wang, X., Sun, H. H., & Van de Water, J. M. (1995). An advanced signal processing technique for impedance cardiography. *IEEE Transactions on Biomedical Engineering*, *42*, 224–230. https://doi.org/10.1109/10.341836

How to cite this article: Forouzanfar M, Baker FC, de Zambotti M, McCall C, Giovangrandi L, Kovacs GTA. Toward a better noninvasive assessment of preejection period: A novel automatic algorithm for B-point detection and correction on thoracic impedance cardiogram. *Psychophysiology*. 2018;55:e13072. https://doi org/10 1111/psyp.13072